Neutrophil dynamics during concurrent chemotherapy and G-CSF administration: Mathematical modelling guides dose optimisation to minimise neutropenia

Morgan Craig[c,e], Antony R. Humphries[b,e,f], Fahima Nekka[e,f], Jacques Bélair[d,e,f], Jun Li[a,e,f], Michael C. Mackey[b,e,g]

[a]*Faculté de Pharmacie, Université de Montréal, Montréal, QC, Canada H3T 1J4*
[b]*Department of Mathematics and Statistics, McGill University, Montreal, QC, Canada H3A 0B9*
[c]*Corresponding author: Faculté de Pharmacie, 3169 Pavillon Jean-Coutu, Université de Montréal, Montréal, QC, Canada H3T 1J4 1.514.343.6111, ext. 1857*
[d]*Département de mathématiques et de statistique, Université de Montréal, Montréal, QC, Canada H3T 1J4*
[e]*Centre for Applied Mathematics in Bioscience and Medicine (CAMBAM), McGill University, Montreal, QC, Canada H3G 1Y6*
[f]*Centre de recherches mathématiques, Université de Montréal, Montréal, QC, Canada H3C 3J7*
[g]*Departments of Physiology and Physics, McGill University, Montreal, QC, Canada H3G 1Y6*

Keywords: myelopoeisis; physiological mathematical modelling; pharmacokinetics/pharmacodynamics

Abstract

The choice of chemotherapy regimens is often constrained by the patient's tolerance to the side effects of chemotherapeutic agents. This dose-limiting issue is a major concern in dose regimen design, which is typically focused on maximising drug benefits. Chemotherapy-induced neutropenia is one of the most prevalent toxic effects patients experience and frequently threatens the efficient use of chemotherapy. In response, granulocyte colony-stimulating factor (G-CSF) is co-administered during chemotherapy to stimulate neutrophil production, increase neutrophil counts, and hopefully avoid neutropenia. Its clinical use is, however, largely dictated by trial and error processes. Based on up-to-date knowledge and rational considerations, we develop here a physiologically-realistic model to mathematically characterise the neutrophil production in the bone marrow which we then integrate with pharmacokinetic and pharmacodynamic (PKPD) models of a chemotherapeutic agent and an exogenous form of G-CSF. In this work, model parameters represent the average values for a general patient and are extracted from the literature or estimated from available data. The dose effect predicted by the model is confirmed through previously published data. Using our model, we were able to determine clinically-relevant dosing regimens that advantageously reduce the number of rhG-CSF administrations compared to original studies while significantly improving the neutropenia status. More particularly, we determine that it could be beneficial to delay the first administration of rhG-CSF to day seven post chemotherapy and reduce the number of administrations from ten to three or four for a patient undergoing 14-day periodic chemotherapy.

URL: morgan.craig@umontreal.ca (Morgan Craig), tony.humphries@mcgill.ca (Antony R. Humphries), fahima.nekka@umontreal.ca (Fahima Nekka), jacques.belair@umontreal.ca (Jacques Bélair), li@crm.umontreal.ca (Jun Li), michael.mackey@mcgill.ca (Michael C. Mackey)

1. Introduction

Mammalian hematopoiesis is an ideal system in which to study the control of cellular proliferation and differentiation. This is because of the rapid division of hematopoietic precursor cells and the morphologically well characterised stages that these cells go through in their progression to mature and functional white cells, red cells and platelets. Just as experimentalists have exploited these characteristics in their laboratory studies, so have biomathematicians utilised this system to sharpen their modelling tools to understand hematological dynamics drawing on a spectrum of clinically interesting diseases in their quest to understand the nature of hematopoietic control [7, 13]. These dynamics include a variety of periodic hematological diseases [7] as well as the observed response of the normal hematopoietic system to periodic perturbation as a side effect of chemotherapy [3, 37].

Chemotherapy is widely used to reduce the spread of malignant cells by interrupting their growth and eventual proliferation. Unfortunately the nonselective nature of chemotherapeutic drugs also disrupts development in non-malignant cell lines, including the blood cells. Neutropenia, a condition characterised by a diminished number of neutrophils, is a common dose-limiting side effect of chemotherapy. In this acute condition, the production of neutrophils in the bone marrow is disrupted. In a healthy individual, circulating neutrophils are created from the commitment of a hematopoietic stem cell (HSC), which undergoes division, maturation, and remain in a reservoir within the bone marrow before being released into the systemic circulation. Patients with low neutrophil counts are susceptible to infection, and to stimulate the production of neutrophils post-chemotherapy, recombinant human granulocyte colony-stimulating factor (rhG-CSF) is administered.

A number of authors have addressed the issue of post-chemotherapy neutropenia through mathematical models, with or without the administration of rhG-CSF (see [3, 8, 9, 19, 31, 35] among others). In this paper, we extend our previous modelling of the regulation of neutrophil dynamics [3, 7, 37] in two significant ways. First we take into account the sequestering of mature neutrophils into a reservoir in the bone marrow before their release into circulation. Secondly, we account for the marginated pool of neutrophils in the blood. Finally, we include a physiologically realistic representation of the action of a recently developed chemotherapeutic drug (Zalypsis), and extend our previous models for the effects of rhG-CSF. These extensions to previous work on neutrophil dynamics, combined with our determination of relevant model parameters from the physiological and clinical literature, have led to a model that is physiologically realistic. That this is the case is evidenced by the fact that the model reproduces recently published data on the temporal neutrophil response in a population of 172 patients receiving periodic chemotherapy every 14 days *without any parameter fitting*. Furthermore, using this extended model for neutrophil regulation we have examined the response of the model to the administration of rhG-CSF following simulated chemotherapy. We predict that a significant reduction (from 10 to 3 or 4) in the number of days of administration of rhG-CSF will still result in a clinically satisfactory outcome. If this prediction is borne out in a clinical setting it will have a significant impact on the cost of post-chemotherapy treatment.

This paper is structured as follows: Section 2.1 provides the motivation and details the construction of the myelopoiesis model by updating our group's previously published works ([3, 5] and [8]). Section 2.2 develops the pharmacokinetic models for both the chemotherapeutic drug zalypsis and rhG-CSF (filgrastim) which have been adapted from previously developed models (particularly [11] and [17]). The hematopoietic effect of both drugs is modelled in Section 2.3.1. Results are presented in Section 3, where the model is first validated against published data on a population of 172 patients receiving chemotherapy (Section 3.2.1) and then used to examine dose optimisation (Section 3.2.2). The paper concludes with a discussion of our findings in Section 4. Details on the estimation of model parameter from the physiological and clinical literature are to be found in the Appendix.

2. The Model

2.1. Development of a Physiological Model of Granulopoiesis

In the following, the reader may find it useful to refer to the schematic representation of neutrophil production in Figure 1. The production of a single neutrophil from an HSC in the bone marrow can be summarised into five distinct steps: differentiation, proliferation, maturation, sequestration, and exit, whether by random loss or through entry into the blood stream/tissues. Once in circulation, neutrophils die at random through apoptosis. The physiological model we present here is an extension of previously proposed models ([3, 8] and [19]), with the notable addition of a mature neutrophil reservoir that holds newly mature neutrophils in the bone marrow so the body may react rapidly in the case of falling neutrophil blood counts or infection [10, 30]. Our model also differs from the models in [3, 8] and [19] by accounting for the difference in the sizes of the total blood neutrophil pool and the circulating neutrophil pool caused by margination in the blood.

The production of circulating neutrophils begins with the hematopoeitic stem cells (HSCs, population Q in units of 10^6 cells/kg). The HSCs are generally considered to be in the quiescent stage, though they may enter the proliferative stage at rate β (days^{-1}) for a period of τ_S (days), differentiate into the neutrophil line at a rate $\kappa_N(N)$ (units days^{-1}), or enter the erythroid or platelet lineages at a rate of κ_δ (days^{-1}). The HSCs undergo apoptosis at rate γ_S (days^{-1}) during their proliferative phase and their total amplification during their proliferative phase is given by $A_Q(t)$ (Equation (6)). Once committed to the neutrophil lineage, cells divide at rate η_{NP} (days^{-1}) before entering a maturing phase with variable aging velocity $V_N(t)$ where they remain for a period of $\tau_{NM}(t)$ days. Upon beginning the maturation process, neutrophil precursors grow in volume but are no longer proliferating and experience random cell death at a rate of γ_{NM} (days^{-1}). The total amplification of committed precursors is $A_N(t)$ (see Equation (7)). Once mature, cells do not exit the bone marrow directly but are sequestered into a reservoir pool (population N_r in units of 10^9 cells/kg) and a steady stream of reserved, mature neutrophils transition into the blood with rate $f_{trans}(G(t))$ (in units of days^{-1}) which depends on the circulating concentration of G-CSF ($G(t)$ in ng/mL). Indeed, in the case of reduced circulating numbers or infection, G-CSF concentrations rise and mature neutrophils are rapidly mobilised from the reserve pool.

Cells that do not reach the blood exit the reservoir pool at a rate γ_{Nr} (days^{-1}). Neutrophils in the blood may be circulating or marginated. We let N (in units of 10^9 cells/kg) be the size of the total blood neutrophil pool (TBNP) which is composed of both the circulating neutrophil pool (CNP) and the marginated neutrophil pool (MNP). We assume free exchange and identical kinetics in the CNP and MNP, and also that the ratio of their sizes is constant over time. Neutrophils (population N in units of 10^9 cells/kg) are then removed from the TBNP at a rate of γ_N days^{-1}. This implies that the average lifespan of a neutrophil within the TBNP is $1/\gamma_N$. Overall, the time from the entrance of a stem cell into the neutrophil line to the exit of progeny into the blood is $\tau_N = \tau_{NP} + \tau_{NM}(t)$ (days).

The entire process of granulopoiesis is regulated by G-CSF, which stimulates entry into the neutrophil lineage, promotes proliferation, speeds up maturation, and increases mobilisation from the reservoir pool. The circulating neutrophils and the concentration of G-CSF are under constant feedback control so the concentration of G-CSF is increased when neutrophil counts decrease, thereby stimulating the production of more neutrophils to be released into the circulation which, in turn, reduces G-CSF levels.

In our model, the production of neutrophils is described by a system of three differential equations describing the temporal evolution of hematopoeitic stem cells ($Q(t)$), the mature neutrophil reservoir pool in the marrow ($N_r(t)$), and the total blood neutrophil pool ($N(t)$). Two of these differential equations involve delays and so the model is described by a system of delay differential equations (DDEs). The equations are derived from an age-structured partial differential equation (PDE) model with appropriate boundary conditions. Careful attention must be paid here to the derivation of the DDEs from the PDEs due to the dependency of the maturation speed upon G-CSF, implying that we are dealing with an age-structured model with variable aging rate and threshold maturation condition. A detailed derivation can be found in [14] and explanations of all of the parameters can be found in Table 1.

The model's equations are given by

$$\frac{dQ(t)}{dt} = -\left(\kappa_N(N(t)) + \kappa_\delta + \beta(Q(t))\right) Q(t) + A_Q(t)\beta\left(Q(t-\tau_S)\right) Q(t-\tau_S) \tag{1}$$

$$\frac{dN_r(t)}{dt} = A_N(t)\kappa_N(N(t-\tau_N))Q(t-\tau_N)\left(\frac{V_N(G(t))}{V_N(G(t-\tau_{NM}(t)))}\right) - \Big(\gamma_{Nr} + f_{trans}(G(t))\Big)N_r(t) \tag{2}$$

$$\frac{dN(t)}{dt} = f_{trans}(G(t))N_r(t) - \gamma_N N(t), \tag{3}$$

subject to the initial condition of homeostasis ($Q(t) = Q^{homeo}$, $N_r(t) = N_r^{homeo}$, $N(t) = N^{homeo}$, for all $t \le t_0$, where t_0 marks the beginning of treatment). In our model $N(t)$ represents the total blood neutrophil pool (TBNP). If we are interested in only circulating neutrophil numbers for comparison with clinical measurements, we simply multiply $N(t)$ by the fraction of circulating cells. This calculation is detailed in Section 4.

Neutrophils are relatively large and have long transit times through smaller capillaries, particularly in the lungs and spleen, which largely results in their nonuniform distribution in the blood, and the difference in the size of the circulating neutrophil pool (CNP) as measured from blood samples, and the TBNP. In the models of [3, 8] and [19] the

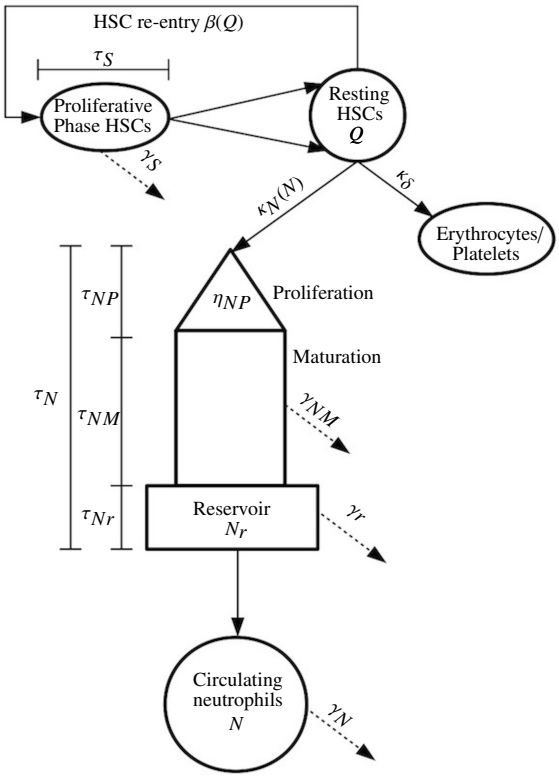

Figure 1: Schematic representation of the production of circulating neutrophils in the bone marrow. Stem cells (Q) undergo the usual cell cycle and mitosis (at rate $\beta(Q)$) where they die at rate γ_S or return to the quiescent stage. They then remain at rest until differentiation into the neutrophil lineage (at rate $\kappa_N(N)$) or other blood lines at rate κ_δ. After entering the neutrophil lineage, a period of successive divisions (proliferation) at rate η_{NP} is followed by a maturing phase with velocity V_N. The mature neutrophils then reach the neutrophil reservoir (N_r) in the bone marrow. Mature reserved cells are maintained within the bone marrow for rapid mobilisation if needed [10]; the rate of transfer from the pool into the circulation (f_{trans}) is determined by G-CSF concentrations in the central compartment (plasma). Mature reserved neutrophils that do not reach the circulation die from the reservoir at rate γ_{Nr}. Circulating neutrophils N disappear from the circulation by apoptosis at rate γ_N. The time for the hematopoietic stem cell proliferative phase cycle is τ_S. The process of the development of a neutrophil takes time τ_N from their entry into the neutrophil line to their appearance in the blood, which includes the time for proliferation (τ_{NP}), maturation (τ_{NM}), and marrow sequestration (τ_{Nr}).

quantity $N(t)$ was taken to directly represent the CNP, but like us they modelled the total production of neutrophils in the bone marrow. However, since the size of the CNP is significantly smaller than the TBNP, and the models in [3, 8] and [19] required very large apoptosis rates in the maturation phase of the neutrophils. Essentially, in those models the neutrophils that should have been destined for the marginated neutrophil pool (MNP) in the blood were instead removed from the maturation phase by apoptosis, since those models contained no MNP for those cells to enter. By letting $N(t)$ represent the total blood neutrophil pool in the current model we avoid the necessity of artificially elevated apoptosis rates in the maturation phase and mature neutrophil reservoir pool.

In the current model above, we have that

$$\beta(Q) = f_Q \frac{\theta_2^{s_2}}{(\theta_2^{s_2} + Q^{s_2})} \tag{4}$$

$$\kappa_N(N) = f_N \frac{\theta_1^{s_1}}{(\theta_1^{s_1} + N^{s_1})} \tag{5}$$

$$A_Q(t) = 2\exp\left[-\int_{t-\tau_S}^{t} \gamma_S(s)ds\right] \tag{6}$$

$$A_N(t) = \exp\left[\int_{t-\tau_N(t)}^{t-\tau_N(t)+\tau_{NP}} \eta_{NP}(s)ds - \int_{t-\tau_N(t)+\tau_{NP}}^{t} \gamma_{NM}(s)ds\right]. \tag{7}$$

Numerical implementation of the amplification rates of Equations (6) and (7) is obtained by differentiating the integral expressions to obtain the following DDEs

$$\frac{dA_Q}{dt} = A_Q(t)\left[\gamma_S(t-\tau_S) - \gamma_S(t)\right], \tag{8}$$

$$\frac{dA_N}{dt} = A_N(t)\left[\left(1 - \frac{d\tau_N(t)}{dt}\right)\left(\eta_{NP}(t-\tau_N(t)+\tau_{NP}) + \gamma_{NM}(t-\tau_N(t)+\tau_{NP}) - \eta_{NP}(t-\tau_N(t))\right) - \gamma_{NM}(t)\right], \tag{9}$$

where $d\tau_N(t)/dt$ is defined by Equation (24) detailed below (the temporal-evolution of the maturing phase delay depends on the speed of maturation). The initial conditions of Equation (8) and Equation (9) are the homeostatic value of the amplification rates (i.e. A_Q^{homeo} and A_N^{homeo}).

2.2. Pharmacokinetic Modelling

Zalypsis is a cytotoxic agent whose mechanism of action is thought to disrupt the cell cycle and inhibit transcription through binding to cells' DNA [24]. It has been shown to have a significant killing action in several tumour sites *in vivo* while demonstrating strong suppression of proliferation *in vitro* [24]. Population pharmacokinetic (Pop-PK) studies of zalypsis have demonstrated that a four-compartment model is the most appropriate to describe the time-course of its concentration in the blood, implying that the drug is highly distributed in the tissues. Further, it has been determined that zalypsis has but one principal channel of elimination from the central compartment [24]. This same study also concluded that no covariates were linked to the pharmacokinetics of zalypsis, meaning that the physical parameters selected for investigation were not found to influence interindividual variability in the model.

Using the commonly relied-upon transit compartment model of the neutrophil lineage of [9], it has been reported that a power function effects model was sufficient to reproduce the neutropenic effects of zalypsis *in vivo* [11]. The same study also identified two equivalently optimal dosing regimens for the administration of zalypsis, having determined that the incidence and severity of the drug's neutropenic effects were both dose- and frequency-dependent. Owing to this dose-dependency, a more frequent dosing schedule per chemotherapy cycle was determined to be possible providing the total dose remained unchanged. For the phase II clinical trial, the authors recommended a 2.0 mg/m^2 dose be administered over a 1-h infusion three times per 28 day cycle (on days 1, 8, and 15) or as a 4.0 mg/m^2 dose infused over 1-h once every 21 days [11].

Filgrastim is a commercially-available form of rhG-CSF which is used in diverse applications including as an adjuvant to promote neutrophil production during chemotherapy. It acts as endogenous G-CSF but is an unglycosylated molecule which is cleared quickly (half-life of around 3.5 hours) by the kidneys [1]. Its clinical administration is mainly subcutaneous and it is available in two formats (300 μg and 480 μg), implying that administered doses calculated per body weight are rounded to the nearest size to minimise waste [1, 21]. Current dosing protocols state that the administration of filgrastim should begin one day post-chemotherapy and continue until neutrophil counts reach 10 000 mm^{-3} [1], though its clinical use can vary based on institutional practices and may be administered for between 7 to 10 days post-chemotherapy [21].

2.2.1. Zalypsis Pharmacokinetics

As previously mentioned, a four-compartment Pop-PK model of zalypsis was proposed in [11] and [24], implying that drug molecules distribute to and from the plasma into fast-exchange and slow-exchange tissues before inevitably being cleared from the blood. The PK model is given by the following system of ODEs

$$\frac{dC_p}{dt} = \frac{Dose_{Zal}}{\Delta_t} + k_{21}C_{\text{fast}} + k_{31}C_{\text{slow}_1} - (k_{12} + k_{13} + k_{el_C})C_p \tag{10}$$

$$\frac{dC_{\text{fast}}}{dt} = k_{12}C_p + k_{42}C_{\text{slow}_2} - (k_{21} + k_{24})C_{\text{fast}} \tag{11}$$

$$\frac{dC_{\text{slow}_1}}{dt} = k_{13}C_p - k_{31}C_{\text{slow}_1} \tag{12}$$

$$\frac{dC_{\text{slow}_2}}{dt} = k_{24}C_{\text{fast}} - k_{42}C_{\text{slow}_2}, \tag{13}$$

where C_p is the systemic concentration of zalypsis (traditionally referred to as the central or first compartment), C_{fast} is the concentration of zalypsis in the fast-exchange tissues (second compartment), and C_{slow_1} and C_{slow_2} are the concentrations in the slow-exchange tissues (third and fourth compartments, respectively), k_{ij} are constants expressing the rate of transfer between the i^{th} and j^{th} compartments, and k_{el_C} is the rate of elimination from the central compartment. As is typical in PK studies, this rate of elimination can be expressed as $k_{el} = \frac{Cl}{V_1}$, or the rate of clearance Cl over the volume of the central compartment V_1. The rate of IV infusion of zalypsis is the division of the IV dose ($Dose_{Zal}$) by the duration of the infusion Δ_t (typically one hour).

2.2.2. G-CSF Pharmacokinetics

We express the changes in concentration of circulating G-CSF by accounting for G-CSF concentrations entering the blood stream ($G(t)^{in}$) and G-CSF concentrations exiting the blood stream ($G(t)^{out}$) per unit time

$$\frac{dG(t)}{dt} = \frac{dG(t)^{in}}{dt} - \frac{dG(t)^{out}}{dt},$$

where

$$G(t)^{in} = G(t)^{endo} + G(t)^{admin}$$
$$G(t)^{out} = R^{ren} + R^{int}.$$

The endogenous production rate of G-CSF is believed to be constant [12, 15], implying that

$$G(t)^{endo} = G_{prod},$$

where G_{prod} (in ng/mL/day) is the zero-order rate of endogenous production. In oncological settings, rhG-CSF is administered subcutaneously and several authors have proposed models for fractionated absorption after subcutaneous administration (see, for example, [23] and [27]). We selected the model of [17], which neglects a subcutaneous pool compartment in favour of a decreasing exponential rate of diffusion from the subcutaneous tissue, because it did not introduce additional compartments to the filgrastim model:

$$G(t)^{admin} = \frac{k_a F(Dose_{GCSF})}{V_d} e^{-k_a t_{inj}}. \tag{14}$$

Through the term $e^{-k_a t_{inj}}$ (t_{inj} being the time since the subcutaneous injection), the amount of rhG-CSF absorbed from the subcutaneous pool decreases with increasing time. Here F is the bioavailable fraction, $Dose_{GCSF}$ is the administered dose (ng), k_a is the absorption constant (days^{-1}), and V_d is the volume of distribution (mL).

The removal of G-CSF from the body is accomplished through two mechanisms: by renal elimination and through binding and internalisation by the neutrophils [3, 18]. We account for the renal elimination with

$$R^{ren} = k_{ren} G(t),$$

where k_{ren} is the first-order rate constant of renal elimination. The internalisation of G-CSF by the neutrophils is modelled using the Hill equation for receptor-complex formation. Since G-CSF binds to neutrophil receptor sites with a 2:2 stochiometry [18], the Hill coefficient for the receptor dynamics is taken to be 2. We then have

$$R^{int} = k_{int} \frac{G^2(t)}{(G^2(t) + K_D^2)} N(t), \tag{15}$$

where k_{int} is the rate of internalisation and K_D is the usual dissociation constant. Hence

$$G(t)^{in} = G_{prod} + \frac{k_a F(Dose_{GCSF})}{V_d} e^{-k_a t_{inj}}$$
$$G(t)^{out} = k_{ren} G(t) + k_{int} \frac{G^2(t)}{(G^2(t) + K_D^2)} N(t)$$

and, finally, the model for the pharmacokinetics of G-CSF is given by

$$\frac{dG(t)}{dt} = \frac{k_a F(Dose_{GCSF})}{V_d} e^{-k_a t_{inj}} + G_{prod} - k_{ren} G(t) - \chi k_{int} \frac{G(t)^2}{(G(t)^2 + K_D^2)} N(t), \tag{16}$$

where $\chi = G^{homeo}/N^{homeo}$ (with G^{homeo} the homeostatic concentration of G-CSF and similarly for N^{homeo}) is a normalisation factor necessary to obtain the equilibrium at homeostatic conditions (absence of rhG-CSF administration–refer to the Appendix).

2.3. Determination of Pharmacodynamic Models for Drug Effects

Generally speaking, the usual empirical Michaelis-Menten and Hill equations serve to model most PD effects in this section.

2.3.1. Myelosuppressive Effects of Chemotherapy

Since chemotherapy usually acts to disrupt cellular division, we assume that the systemic concentration of the chemotherapeutic agent affects only proliferating cells. This implies that the death rate of the proliferating stem cells will increase during administration of chemotherapy. To our knowledge, no studies report the direct effects of chemotherapy on the hematopoietic stem cells, so we retain, for simplicity, a linear model for the PDs of zalypsis on the population Q [3]. Accordingly, we model the increase in the death rate for the stem cells during chemotherapy as

$$\gamma_S^{chemo}(C_p(t)) \quad = \quad \gamma_S^{homeo} + h_S C_p, \tag{17}$$

where γ_S^{chemo} relates the effect of chemotherapy on the rate of apoptosis in the proliferative HSCs through the increase of γ_S^{homeo} (the homeostatic rate of apoptosis of the proliferative HSCs) by the effect h_S of the plasma concentration of the chemo-agent.

Concurrently, the rate of proliferation of the neutrophils in the bone marrow will decrease during exposure to chemotherapeutic agents. To model this effect, we modified the usual Imax (inhibitory Michaelis-Menten) PD model given by

$$E = \frac{E_{max} C_p^h}{EC_{50}^h + C_p^h}$$

to incorporate the two main assumptions on the effects of chemotherapy on the neutrophil proliferation rate. In the above equation, E is the observed effect, E_{max} is the maximal observed effect, C_p is the plasma concentration of the drug, EC_{50} is the concentration of drug inducing 50% of the maximal effect, and h is the usual Hill coefficient which determines the slope of the concentration-effects curve.

For our purposes, we consider that neutrophil proliferation would be completely halted when the plasma concentration of the chemotherapeutic agent is at a maximum (at supra-therapeutic levels, so $C_p^\infty \gg EC_{50}$, , where C_p^∞ is an intolerably high dose of continuous chemotherapy). This implies that $\eta_{NP}^{chemo}(C_p^\infty) = 0$. Further, when no chemotherapy is given ($C_p(t) = 0$), the proliferation rate remains at the steady state homeostatic rate, so that $\eta_{NP}^{chemo}(0) = \eta_{NP}^{homeo}$, where η_{NP}^{homeo} is the homeostatic rate of neutrophil proliferation. Together, these conditions imply that the above Imax model is instead expressed as

$$\eta_{NP}^{chemo}(C_p(t)) \quad = \quad \eta_{NP}^{homeo}\left(\frac{(EC_{50})^h}{(EC_{50})^h + \left(C_p(t)\right)^h}\right). \tag{18}$$

2.3.2. Myelostimulative Effects of G-CSF

Following [7, 32, 36], G-CSF reduces cell death rates in the HSCs and the random loss rates of the maturing neutrophils (decreasing γ_S and γ_{NM}, respectively) while also increasing the rate of proliferation of the marrow neutrophils (increasing η_{NP}). In what follows, the b_i, $i = S, N, NP, V$ are parameters relating the half-maximal concentration of G-CSF (see the Appendix for details on the estimation of these parameters). We consider the death rate out of the neutrophil marrow reservoir γ_{Nr} to be constant for simplicity. The rate of loss of the HSCs is given by

$$\gamma_S(G(t), C_p(t))) \quad = \quad \gamma_S^{min} - \frac{(\gamma_S^{min} - \gamma_S^{chemo})b_S}{G(t) - G^{homeo} + b_s}, \tag{19}$$

and is subject to the simultaneous effects of the chemotherapy and G-CSF in the stem cell compartment acting as an indirect feedback loop from the circulating neutrophil numbers. Here, γ_S^{min} is the minimal rate of apoptosis in the HSCs proliferative phase. The effects of G-CSF on cells committed to the neutrophil lineage are expressed as

$$\eta_{NP}(G(t), C_p(t)) \quad = \quad \eta_{NP}^{chemo}(C_p(t)) + \frac{(\eta_{NP}^{max} - \eta_{NP}^{chemo}(C_p(t)))(G(t) - G^{homeo})}{G(t) - G^{homeo} + b_{NP}} \tag{20}$$

$$\gamma_{NM}(G(t)) \quad = \quad \gamma_{NM}^{min} - \frac{(\gamma_{NM}^{min} - \gamma_{NM}^{homeo})b_{NM}}{G(t) - G^{homeo} + b_{NM}}, \tag{21}$$

where η_{NP}^{max} is the maximal proliferation rate of the neutrophils and γ_{NM}^{min} is the minimal rate of random cell loss of the maturing neutrophils. As is the case for the HSCs, the proliferation rate $\eta_{NP}(G(t), C_p(t))$ is subject to the simultaneous effects of chemotherapy and G-CSF. Additionally, it is known that visibly immature neutrophils appear in the circulation after exogenous G-CSF administration [30]. Since our system is a DDE model with variable aging rate, we express this effect by a dependency of the maturation time on G-CSF (decreasing $\tau_{NM}(t)$), which implies an increase in the speed of maturation (increasing $V_N(t)$) modelled by

$$V_N(G(t)) \quad = \quad 1 + (V_{max} - 1)\frac{G(t) - G^{homeo}}{G(t) - G^{homeo} + b_V}, \tag{22}$$

where V_{max} is the maximal aging velocity of the maturing neutrophils (see the Appendix). The maturation time $\tau_{NM}(t)$ is defined by the threshold condition

$$\int_{t-\tau_{NM}(t)}^{t} V_N(G(s))ds \quad = \quad a_{NM}, \tag{23}$$

where a_{NM} is a constant equal to the maturation time at homeostasis. Differentiating Equation (23) gives

$$\frac{d\tau_N(t)}{dt} = \frac{d\tau_{NM}(t)}{dt} \quad = \quad 1 - \frac{V_N(G(t))}{V_N(G(t - \tau_{NM}(t)))}. \tag{24}$$

Finally, the concentration of G-CSF determines the mobilisation of mature neutrophils in the marrow reserve into the circulation. The functional form of this effect was previously proposed in [31] and has been generalised here to be

$$f_{trans}(G(t)) \quad = \quad trans^{homeo}\frac{trans^{ratio}(G(t) - G^{homeo}) + b_G}{G(t) - G^{homeo} + b_G}. \tag{25}$$

The parameter $trans^{homeo}$ relates the homeostatic rate of transit from the neutrophil bone marrow reservoir into the circulation. This rate of exit can, under changing G-CSF concentrations, be either increased or decreased by an empirically determined ratio $trans^{ratio} = \frac{trans^{max}}{trans^{homeo}}$, so more neutrophils exit the reservoir into the circulation under higher G-CSF concentrations.

3. Results

Parameter values, their interpretation, units as well as sources of references are reported in Table 1. Parameter estimation can be found in the Appendix.

Parameter	***Interpretation***	***Value***	***Unit***	***Reference***
Stem cells				
Q^{homeo}	Concentration of HSCs at homeostasis	1.1	10^6 cells/kg	[2, 19]
γ_S	HSC rate of apoptosis	0.1	days^{-1}	[3]
τ_S	Time for HSC re-entry	2.8	days	[3, 19, 20]
A_Q^{homeo}	HSC amplification at homeostasis	1.5116		* Eq. (8)
κ_δ	HSC differentiation rate into other lineages	0.0140	days^{-1}	* Eq. (1)
β_Q^{homeo}	HSC rate of re-entry	0.043	days^{-1}	[20]
f_Q	Maximal HSC re-entry rate	8	days^{-1}	**
s_2	HSC re-entry Hill coefficient	2		**
θ_2	Half-maximal HSC concentration	0.0809	10^6 cells/kg	* Eq. (4)
Neutrophils				
N_r^{homeo}	Homeostatic concentration of neutrophil reservoir	2.26	10^9 cells/kg	[6]
N^{homeo}	Homeostatic concentration of total neutrophil pool	0.3761	10^9 cells/kg	[6]
N_{circ}^{homeo}	Homeostatic concentration of circulating neutrophils	0.22	10^9 cells/kg	[6]
γ_N	Circulating neutrophil rate of removal	2.1875	days^{-1}	*
τ_{NP}	Time for neutrophil proliferation	7.3074	days	*
a_{NM}	Time for neutrophil maturation at homostasis	3.9	days	** [28]
τ_{Nr}	Time spent in marrow reserve	2.7	days	**
γ_{Nr}	Rate of removal from marrow reserve	0.0064	days^{-1}	* Eq. (A3)
γ_{NM}	Rate of removal during maturation phase	0.1577	days^{-1}	* Eq. (2)
$\kappa_N(N^{homeo})$	HSC differentiation rate into neutrophil line	0.0073	days^{-1}	** Eq. (A1)
A_N^{homeo}	Neutrophil amplification at homeostasis	103 780		* Eq. (9)
η_{NP}^{homeo}	Neutrophil proliferation rate	1.6647	days^{-1}	*

(=Calculated, **=Estimated) Continued on next page*

Table 1 – *Continued from previous page*

Parameter	***Interpretation***	***Value***	***Unit***	***Reference***
f_N	Maximal rate of neutrophil differentiation	0.0088	days^{-1}	**
s_1	Neutrophil differentiation Hill coefficient	2		[18]
θ_1	Half maximal concentration neutrophil differentiation	0.8409	10^9 cells/kg	* Eq. (5)
f_{trans}^{homeo}	Homeostatic rate of transit from marrow reserve	0.3640	days^{-1}	* Eq. (5)
Zalypsis				
k_{el_C}	Zalypsis rate of elimination	132.0734	days^{-1}	[24]
k_{12}	Rate of exchange	90.2752	days^{-1}	[24]
k_{21}	Rate of exchange	18.2222	days^{-1}	[24]
k_{13}	Rate of exchange	8.2936	days^{-1}	[24]
k_{31}	Rate of exchange	0.6990	days^{-1}	[24]
k_{24}	Rate of exchange	9.2296	days^{-1}	[24]
k_{42}	Rate of exchange	62.5607	days^{-1}	[24]
BSA	Average body surface area	1.723	m^2	[24]
G-CSF				
G^{homeo}	G-CSF concentration at homeostasis	0.0246	ng/mL	[17]
G_{prod}	Rate of G-CSF production	0.2535	ng/mL/days	* Eq. (16)
k_{ren}	Rate of G-CSF renal elimination	10.3	days^{-1}	[31]
χ	Normalisation factor	0.0654	$(\text{ng/mL})/(10^9\text{cells/kg})$	**
k_{int}	G-CSF receptor-internalisation rate	114.48	days^{-1}	[31]
k_D	G-CSF dissociation constant	1.44	ng/mL	[17]
k_a	Subcutaneous filgrastim absorption rate	13.5	days^{-1}	[31]
F	Filgrastim bioavailable fraction	0.6020		[17]
V_d	Volume of distribution (filgrastim)	1788	mL	* [17, 31]
PD parameters				
Chemotherapy				
γ_S^{homeo}	HSC apoptotic homeostatic rate	0.1	days^{-1}	[3]
γ_S^{min}	Minimal HSC apoptotic rate	0.1	days^{-1}	[3]
γ_S^{max}	Maximal HSC apoptotic rate	0.4	days^{-1}	[3]
h_S	First-order effect of chemotherapy on HSC apoptosis	0.1		**
b_S	HSC apoptosis Michaelis-Menten parameter	11.2679	ng/mL	* Eq. (A6)
h	Hill coefficient for zalypsis effect on proliferation	3		[29]

(=Calculated, **=Estimated)* *Continued on next page*

Table 1 – *Continued from previous page*

Parameter	***Interpretation***	***Value***	***Unit***	***Reference***
EC_{50}	Zalypsis half-concentration on proliferation	2.3056	ng/mL	[29]
G-CSF				
η_{NP}^{max}	Maximal rate of proliferation	2.544	days^{-1}	[3]
η_{NP}^{min}	Minimal rate of proliferation	0.4	days^{-1}	[3]
V_{max}	Maximal maturation velocity	10	days^{-1}	* [28]
γ_{NM}^{min}	Minimal apoptosis rate out of maturing phase	0.12	days^{-1}	[3]
γ_{NM}^{max}	Minimal apoptosis rate out of maturing phase	0.67	days^{-1}	[3]
$trans^{max}$	Maximal rate of transfer from marrow reserve	1.456	days^{-1}	[32]
b_V	Michaelis-Menten parameter (maturation speed)	3.5	ng/mL	* [28]
b_{NP}	Michaelis-Menten parameter (proliferation)	11.2679	ng/mL	* Eq. (A6)
b_{NM}	Michaelis-Menten parameter (maturation)	11.2679	ng/mL	* Eq. (A6)
b_G	Michaelis-Menten parameter (transit from pool)	11.2679	ng/mL	* Eq. (A6)

Table 1: Table of parameter values used for an average patient undergoing chemotherapy with filgrastim support.

3.1. Numerical Simulations

The mathematical modelling of hematopoiesis, zalypsis, and filgrastim was supplemented by numerical simulation. All models were simulated using the *ddesd* solver in Matlab [22], which is an adaptive Runge-Kutta solver for DDEs with state-dependent delays. Since our model's delays are explicitly physiological and not artificially imposed by the modelling structure, defining several parameters in our model required extrapolation from published neutrophil studies, particularly [4] and [6]. Some digitisation was carried out using Matlab to facilitate the estimation.

3.2. The Use of Physiologically-based Models

The regulation of myelopoiesis is a dynamical system which implies that any periodic administration of a perturbation (for our purposes, chemotherapy) can induce oscillations where there were none previously. Additionally, in a phenomenon known as resonance [3], the cyclical administration of myelosuppressive chemo-agents can worsen the neutrophil nadir when administered during specific periods in the oscillating cycle. We therefore sought to study how a periodic chemotherapeutic regimen affects neutrophil counts and how the timing of the administration of filgrastim post-chemotherapy influences the patient's neutropenic status. This combines previous work addressing the effects of period-shortening in poly-chemotherapy ([25, 26]; Section 3.2.1–see below) and dose optimisation to minimise neutropenia during treatment with zalypsis [11].

3.2.1. Verifying the Model's Predictions

CHOP21, an established treatment for lymphoma, involves the concomitant administration of cyclophosphamide, doxorubicin, vincristine, and prednisone given over 21-day cycles, with G-CSF administration determined *ad libitum* by the individual patient's neutrophil count. Investigations into period-condensing in the CHOP protocol (14-day instead of 21-day) have concluded that a shorter cycle length leads to better survival rates in younger patients (less than 60 years old) and less toxicity in older patients [25, 26]. The CHOP14 14-day protocol calls for G-CSF administration (300 μg/day or 480 μg/day depending on the patient's body weight) to begin 4 days post-chemotherapy and to continue until day 13 post-chemotherapy (for a total of 10 days). Recent work on model development for granulopoiesis has made available extensive data sets from the initial CHOP14 studies [16]. Reported are patients' absolute neutrophil count (ANC) in quartiles for a 6-cycle CHOP treatment, thereby giving an idea of the variability in patients' response to chemotherapy with pre-defined G-CSF support.

Our focus was to compare our model's predictions using a previously optimised dose of zalypsis for a 21-day cycle (4 mg/m^2) to the CHOP14 protocol in a manner analogous to the investigations of [25] and [26]. While it may seem counterintuitive to compare mono- and polytherapies, it is important to note that in the context of our fully mechanistic model, myelosuppressive drugs will have similar effects on the renewal rate of the HSCs ($\beta(Q)$) and on the proliferation rate of the neutrophils ($\eta(G(t), C_p(t))$) since chemotherapeutics drugs are explicitly administered for their ability to disrupt cellular division. Moreover, we were limited by the availability of data in the literature and, as such, made use of the data sets at our disposal (accessed through [16]). Accordingly, we simulated six 14-day period administrations of 4 mg/m^2 of zalypsis with 10 daily administrations of 300 μg of subcutaneous filgrastim beginning on the fourth day post-chemotherapy, as was prescribed for the CHOP14 study. We then compared the model prediction to the CHOP14 data (available in quartiles), which is highlighted in Figure 2. It should be noted here that no parameter fitting was undertaken from clinical data. The values of all constants in the model were determined per published PK models for zalypsis or filgrastim or from physiological studies of neutrophil production. Our simulated result falls within the interquartile ranges from [25, 26] through simple comparison.

3.2.2. Applying the Model to Dose Optimisation

As previously mentioned, the utility of fully mechanistic models is related to their ability to explain and unravel how the underlying physiological mechanisms dictate a drug's effects and efficacy. In parallel, physiologically-based models should afford predictive abilities and help guide dosing decisions. Based on the results depicted in Figure 2, we used our model to optimise the administration of rhG-CSF post-chemotherapy using the CHOP14 chemotherapy protocol (6 cycles of chemotherapy administered 14 days apart with 10 administrations of 300 μg of filgrastim beginning 4 days post-chemotherapy) as a baseline reference case. To ensure clinical relevancy, optimal regimens were labelled as those which reduce the number of administrations of filgrastim over each chemotherapy cycle while simultaneously maintaining or, even better, increasing the ANC nadir observed in the complete CHOP14 study.

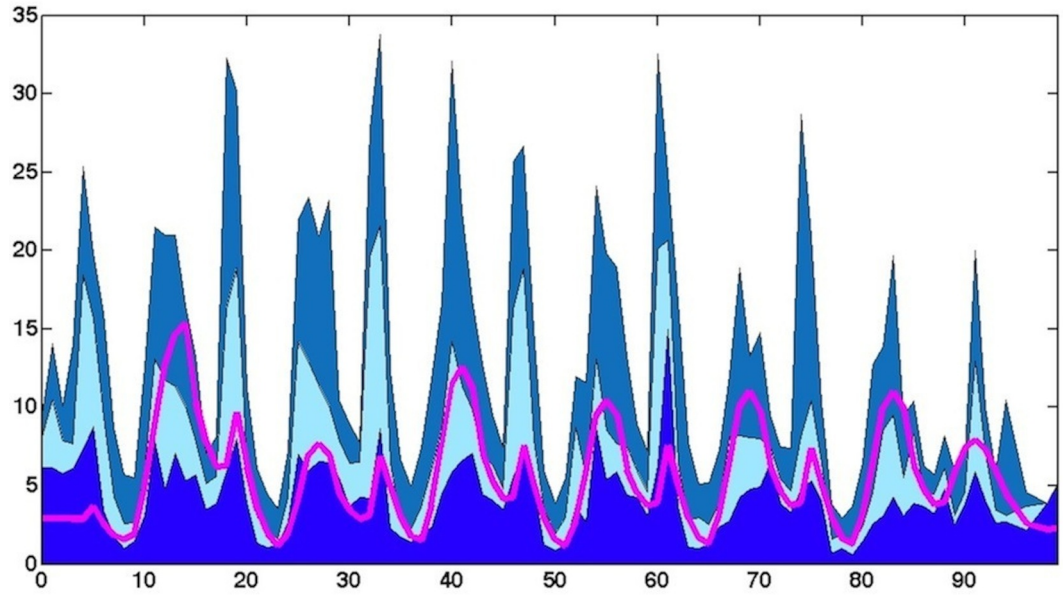

Figure 2: Model predictions (pink) compared to CHOP14 protocol described in [25, 26] (data in quartiles from [16]–shaded regions). x-axis: time (days); y-axis: ANC (10^9 cells/L). The CHOP14 protocol outlined in [25] is compared to the model's prediction. Data from the CHOP14 study available from [16] is divided into quartiles (shaded regions). The simulation results (in pink) shows the model's solution for the typical patient (sampled at clinical sampling points-once daily for 100 days) and compares positively to the study's findings.

To establish optimal dosing regimens, we simulated a baseline standard by administering 4 mg/m^2 dose of zalypsis (previously determined to be an optimal dose for zalypsis [11]) every 14 days for 6 cycles in total. Next we ran simulations in the $(t_{post-chemo}, n_{admins}, p_{admins})$-space by varying both start day ($t_{post-chemo}$), the number of filgrastim administrations (n_{admins}), and the period between filgrastim doses (p_{admins}–up to a maximum of 3 days to minimise the impact of the filgrastim period upon adherence). We then progressively ranked each $(t_{post-chemo}, n_{admins}, p_{admins})$-triplet against the reference by visual predictive check looking for improvement in the ANC nadir.

Our results indicate that the number of administrations of G-CSF post-chemotherapy plays a dominant role on therapeutic outcomes. Indeed, our predictions indicate that the timing of the first administration of G-CSF post-chemotherapy becomes less important when the number of administrations are increased within each chemotherapy cycle (Figures 3 and 4). This supports the current clinical dosing scheme of G-CSF in oncological settings which begins one-day post-chemotherapy and continues daily for seven to ten days, depending on the ANC status of the patient [1]. Our results further indicate that administering the first dose of filgrastim seven days post-chemotherapy improves the neutropenic status of the average patient. This is to be expected based on the time it takes to produce and release a mature neutrophil after proliferation has been disturbed by chemotherapy ($\tau_{NM}(t) + \tau_{Nr}$) and supports the findings' of previous modelling work on G-CSF timing [3, 34]. Indeed, starting G-CSF one week after the chemotherapy dose, we demonstrate that as few as three or four daily administrations of G-CSF are sufficient to completely avoid moderate neutropenia (three administrations) or nadirs characteristic of neutropenia altogether (four administrations). Figure 5

reveals that these dosing regimens are optimal in comparison with the CHOP14 protocol, implying a reduction of six to seven G-CSF doses *per chemotherapy cycle*. Such dosing regimens could lead to significant cost reductions and alleviate the physical and hematopoietic burdens on patients undergoing chemotherapy. We determined that daily dosing of filgrastim is preferable over extending the period between administrations: increasing the time between administrations allowed for more severe reductions in ANC (not shown) and would not support patient adherence. This last result is again attributable to the underlying physiology of neutrophil production, as exogenous G-CSF stimulates the release of reserved marrow neutrophils, which in turn increases ANC (an increase which then triggers a decrease in G-CSF concentrations through saturated internalisation and renal elimination). ANC then returns to homeostatic levels after briefly fluctuating above and below the baseline value. When administration periods were increased past one day, ANCs had time to rise and fall between rhG-CSF doses. Once daily administrations of rhG-CSF staved off the rapid decline after peak ANCs because of the frequent dosing and therefore prevented worsening nadirs.

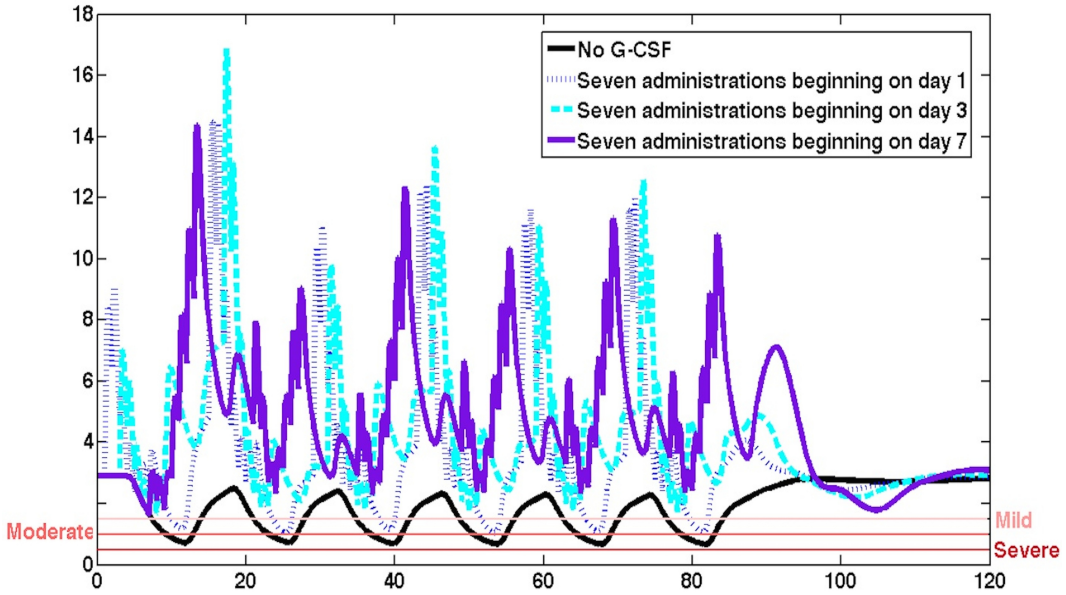

Figure 3: The effect of the day of administration of G-CSF post-chemotherapy. x-axis: time (days); y-axis: ANC (10^9 cells/L). Horizontal lines indicate thresholds for mild (1000 cells/μL $\leq$ ANC $\leq$ 1500 cells/μL), moderate (500 cells/μL $\leq$ ANC $\leq$ 1000 cells/μL), and severe (ANC $\leq$ 500 cells/μL) neutropenia. As the number of administrations of filgrastim post-chemotherapy increase, the importance of the first day of administration diminishes. Six cycles of chemotherapy with 14-day periods are compared for different filgrastim protocols. Seven administrations of filgrastim beginning on day 7 achieve results similar to seven administrations beginning on day 3. A regimen where seven administrations of filgrastim begin 1 day post-chemotherapy is not sufficient to avoid neutropenia.

4. Discussion

In this paper, we have extended an age-structured model for myelopoiesis [3] by the addition of a neutrophil reservoir in the bone marrow that is known to play a role in the rapid mobilisation of neutrophils into the blood during infection

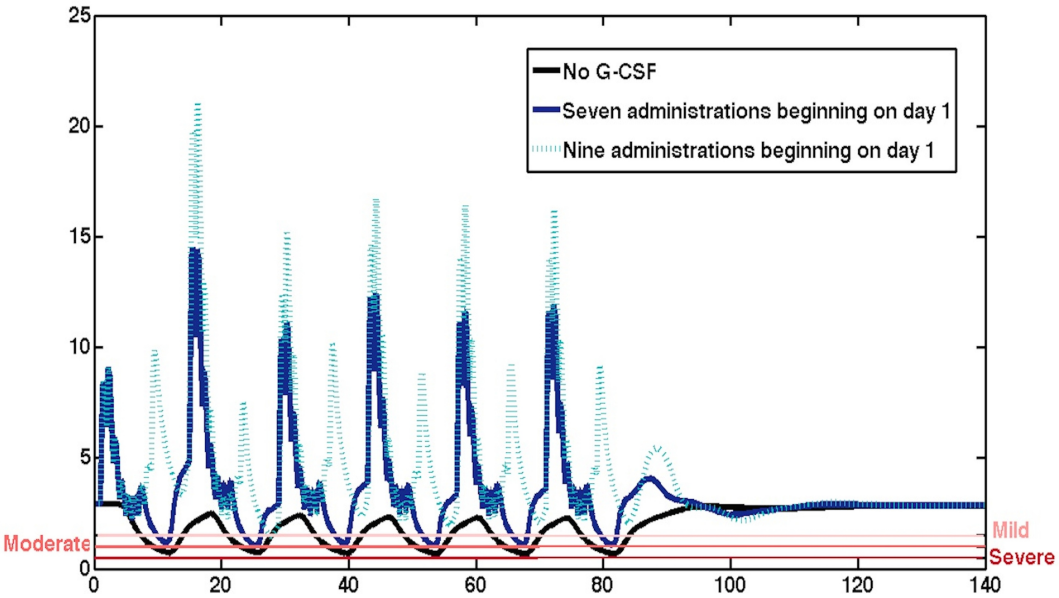

Figure 4: Effect of fixing the starting day post-chemotherapy while increasing the number of G-CSF administrations. x-axis: time (days); y-axis: ANC (10^9 cells/L). Horizontal lines indicate thresholds for mild (1000 cells/μL $\leq$ ANC $\leq$ 1500 cells/μL), moderate (500 cells/μL $\leq$ ANC $\leq$ 1000 cells/μL), and severe (ANC $\leq$ 500 cells/μL) neutropenia. Six cycles of chemotherapy with 14-day periods are compared for different filgrastim protocols. Increasing the number of filgrastim administrations from 7 to 9 allows filgrastim dosing to begin 1 day post-chemotherapy while avoiding neutropenia, which is not the case in the 7 administration regimen, as shown in Figure 3.

or falling circulating neutrophil numbers [10, 30]. We also accounted for the marginated neutrophil pool in the blood. The fully mechanistic physiologically-based model of neutrophil production is then integrated with up-to-date PKPD models for a chemotherapeutic-drug and an adjuvant [17, 24] to characterise the hematopoietic response to periodic chemotherapy with a supportive agent. Parameter estimation was performed in a progressive and logical fashion by establishing the pivotal mechanisms of myelopoiesis from the relevant literature from both physiological studies and PKPD analyses. Proceeding in this manner leads to an improved strategy for parameter identification, one that is capable of evolving in-step with experimental work and physiological knowledge of neutrophil production. Utilising these parameter values directly, the model successfully reproduced the neutrophil data from the CHOP14 studies of 14-day periodic chemotherapy with filgrastim support [25, 26].

We also determined improved dosing regimens for 14-day periodic chemotherapy with the filgrastim adjuvant. We began by studying the optimal timing of the first rhG-CSF dose after the administration of chemotherapy and established that delaying the first dose of filgrastim improved the patient's neutropenic status (Figure 3). This lead us to the determination that the number of filgrastim administrations could be significantly reduced (from 10 to three or four) by delaying its first dose post-chemotherapy (Figure 5). This is a novel result which is simultaneously capable of improving the patient's neutropenic status by raising the neutrophil nadir, of alleviating the patient's drug burden, and of reducing the costs associated with filgrastim support during chemotherapy. It is therefore an important observation

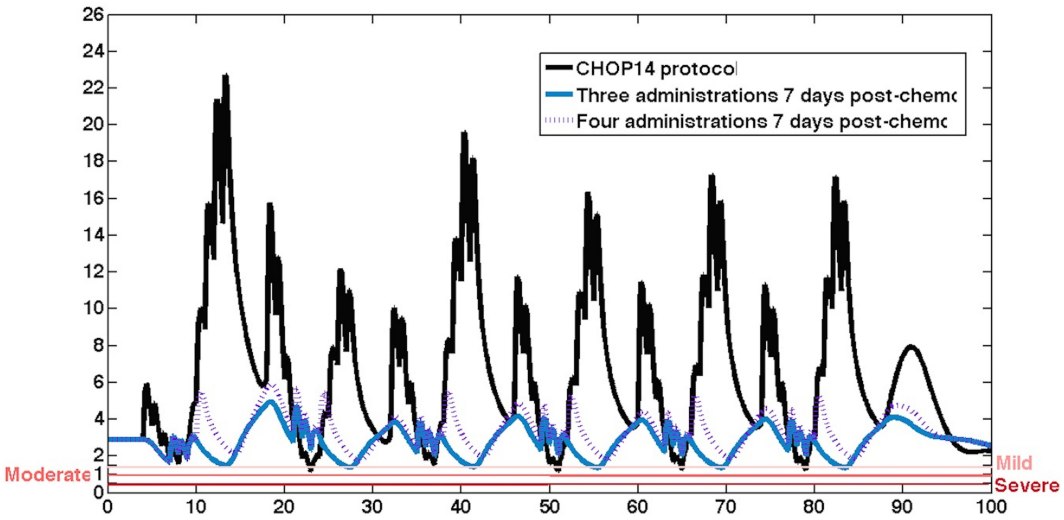

Figure 5: Optimal dosing regimens compared to the CHOP14 protocol. x-axis: time (days); y-axis: ANC (10^9 cells/L). Horizontal lines indicate thresholds for mild (1000 cells/μL $\leq$ ANC $\leq$ 1500 cells/μL), moderate (500 cells/μL $\leq$ ANC $\leq$ 1000 cells/μL), and severe (ANC $\leq$ 500 cells/μL) neutropenia. Model predictions for 6 chemotherapy cycles with 14-day periods. The CHOP14 protocol which studied 10 administrations of filgrastim beginning four days post-chemotherapy is compared to regimens where filgrastim administrations begin seven days post-chemotherapy, with three or four administrations per cycle. Delaying the first administration of filgrastim allows for a reduction in the number of administrations per cycle while showing improvement in the neutropenic status for the average patient.

for the clinical practice and one which bears further investigation through collaboration with clinicians.

Inspired by the results in this paper, we are interested in applying the model to the case of cyclical neutropenia, with the aim of depicting the influence of G-CSF on oscillatory dynamical hematopoietic diseases. Future work will also include a full characterisation of the impact of PK variability in the PD response. Through sensitivity analysis, this depiction will help us discern the principle mechanisms of neutrophil production. Indeed, the rational construction of the myelopoiesis model affords us the ability to delineate the role of individual variables on the predicted behaviour, a particularly salient advantage of physiologically-based models. Outlining which processes significantly impact on myelopoiesis and portraying how these processes affect neutrophil production has implications for patients, clinicians, and researchers alike. This work highlights that hypothesis-driven mathematical modelling contributes considerably to the problem of attenuating chemotherapy-induced neutropenia in the PKPD scope and beyond.

Acknowledgments

This work was supported by the Natural Sciences and Engineering Research Council (NSERC, Canada) PGS-D program (MC), four NSERC Discovery Grants (ARH, JB, MM, FN), and the NSERC Industrial Research Chair in Pharmacometrics (FN), jointly supported by Novartis, Pfizer and inVentiv Health Clinics. We wish to thank Université de Montréal, McGill University, and our colleagues J. Lei (Tsinghua University, China), N. Letarte (Centre hospitalier

de l'Université de Montréal), G. Brooks, G. Provencher Langlois, and L. Ferraton for their insight and support during this project.

Conflicts of Interest/Disclosure

The authors have no conflict of interest to declare. All authors have approved this manuscript.

Author Contributions

This work makes up a portion of the doctoral thesis of MC. Construction of physiological models: MC ARH JB MM. Construction of PKPD models: MC FN JL. Numerical simulation implementation: MC ARH. Data analysis: MC ARH. Wrote the paper: MC FN JL MM ARH.

Appendix

Appendix A: Homeostatic Hematopoietic Parameter Estimation

There are two main points to address in the parameter estimation for the physiological variables. The first issue is interpreting appropriate values from laboratory and clinical studies while the second is assuring that homeostatic levels are consistent when the equations are at steady states. A thorough explanation of the homeostatic parameter values is available in [14]; we will briefly summarise the parameter identification for the hematopoetic values in the absence of chemotherapy and G-CSF and then describe the estimation of parameter values in the PKPD model with both drugs.

We begin with the stem cell line. From [2, 19] we take $Q^{homeo} = 1.1 \times 10^6$ cells/L and set the rate of apoptosis in the stem cell pool to be $\gamma_S = 0.1\,\text{days}^{-1}$ as in [3]. From Equation (6) taken at homeostasis, we have

$$A_Q^{homeo} = 2\exp(-\tau_S \gamma_S) = 1.512.$$

Using an average from the mouse data in [20], we calculate the re-entry rate in the stem cell compartment to be

$$\beta(Q^{homeo}) = \frac{0.02 + 0.053 + 0.057}{3} = 0.043\,\text{days}^{-1}.$$

Clinically determining the rate of differentiation into the neutrophil lineage is difficult and we are not aware of any data estimating this value. Consequently, we use the equilibrium requirement for Equation (1) which gives

$$\kappa_{tot} = (A_Q^{homeo} - 1)\beta(Q^{homeo}) = 0.0220\,\text{days}^{-1}, \tag{A1}$$

where $\kappa_{tot} = \kappa_N(N^{homeo}) + \kappa_\delta$. From this total differentiation rate, we can roughly estimate the differentiation into the neutrophil line as $\frac{1}{3}\kappa_{tot}$, since for our purposes, we consider the hematopoietic stem cells to differentiate into three distinct lineages (neutrophils, red blood cells, and platelets). This implies that $\kappa_N(N^{homeo}) = 0.0073\,\text{days}^{-1}$. From Equation (4), we have

$$\beta(Q^{homeo}) = \frac{f_Q}{1 + \left(\frac{Q^{homeo}}{\theta_2}\right)^{s_2}}. \tag{A2}$$

We take $s_2 = 2$ and $f_Q = 8\,\text{days}^{-1}$, which within the Hill function interpretation can be interpreted to mean that the number of molecules capable of binding to any given stem cell to initiate re-entry is two while the maximal rate of re-entry is $8\,\text{days}^{-1}$ [5]. Rearranging Equation (A2), we get

$$\theta_2 = \left[\frac{(Q^{homeo})^{s_2}\beta(Q^{homeo})}{f_Q - \beta(Q^{homeo})}\right]^{\frac{1}{s_2}} = 0.0809 \times 10^6\,\text{cells/kg}.$$

Turning now to the neutrophil line, from [6], we take the size of the reservoir and total blood neutrophils (respectively) as

$$N_r^{homeo} = 2.26 \times 10^9 \text{ cells/kg}$$
$$N^{homeo} = 0.22/0.585 \times 10^9 \text{ cells/kg}.$$

The factor 0.585 accounts for the reported average recovery rate in [6] and implies that the baseline circulating neutrophil count is 0.22×10^9 cells/kg. From the usual half-life equation for an exponential decay,

$$\gamma_N = \frac{\ln 2}{t_{\frac{1}{2}}} = \frac{35}{16} = 2.1875 \text{ days}^{-1},$$

by rounding the half-life value from [6] of $t_{\frac{1}{2}} = 7.6$ days. At homeostasis, the rate of entry into the reservoir will equal the rate of exit from the pool, giving

$$f_{trans}(G^{homeo})N_r^{homeo} = \gamma_N N^{homeo}$$

or, equivalently,

$$f_{trans}(G^{homeo}) = trans_N^{homeo} = \frac{\gamma_N N^{homeo}}{N_r^{homeo}} = \frac{2.1875 \times 0.4}{2.26} = 0.387.$$

We take $a_{NM} = 3.9$ days which implies, by the constraints detailed in [14], that τ_{Nr}^{homeo} is within the interval $(2.4432, 2.589)$. Accordingly, we select $\tau_{Nr} = 2.5$ days. The average time a neutrophil spends in the reservoir is given by

$$\tau_{Nr}^{homeo} = \frac{1}{f_{trans}(G^{homeo}) + \gamma_{Nr}}, \tag{A3}$$

that is that the average duration of neutrophil within the marrow pool is the reciprocal of the means with which it exits the reservoir: by transiting into the circulation ($f_{trans}(G^{homeo})$) or through random cell death (γ_{Nr}). Rearranging Equation (A3), we have then that the rate of random cell loss from the marrow reserve is

$$\gamma_{Nr} = \frac{1}{\tau_{Nr}^{homeo}} - f_{trans}(G^{homeo})$$
$$= \frac{1}{2.5} - 0.387 = 0.0064 \text{ days}^{-1}.$$

From the age-structured PDE model structure detailed in [14], we determined that $A_N^{homeo} = 103777.178$ and $\eta_{NP}^{homeo} = 1.665 \text{ days}^{-1}$. These values correspond to approximately 17.55 effective divisions within the proliferative phase. We

have also calculated τ_{NP} to be equal to 7.307 days, implying there is one effective division every 10 hours in the proliferative stage [14]. Finally, we can determine the parameters relating to the differentiation rate from the HSCs to the neutrophils. Recall that by Equation (A1), we have set $\kappa_N(N^{homeo}) = \frac{1}{3}\kappa_{tot} = 0.0073\,\text{days}^{-1}$. From this estimate, we calculate the parameters of Equation (5) in a manner similar to Equation (4). From [18], we set $s_1 = 2$ on account of the 2:2 stochiometry between G-CSF and its receptor. We have observed bifurcation from a steady homeostatic equilibrium to a steady limit cycle solution with increases to f_N, which indicates a switch from a hematopoietically normal individual to one exhibiting a pathology similar to cyclical neutropenia [14]. To ensure solutions remain stable at homeostasis, we take $f_N = 1.2\kappa_N(N^*)$. θ_1 is then estimated by

$$\theta_1 = \left[\frac{(N^{homeo})^{s_1}\kappa_N(N^{homeo})}{f_N - \kappa_N(N^{homeo})}\right]^{-s_1} = 0.8409 \times 10^9\,\text{cells/kg}.$$

Appendix B: PK-related Parameter Estimation

All zalypsis parameters are taken directly from [24] and reported in Table 1. An effort was made for G-CSF PK parameter consistency with a number of studies namely [31, 33, 35] and particularly [17]. The endogenous concentration of G-CSF at homeostasis is estimated from [17] as the mean of the observed baseline values in that study, therefore for our purposes, $G^{homeo} = 0.0246\,\text{ng/mL}$. In terms of endogenous production and elimination, we estimated $G_{prod} = 0.2535\,\text{ng/(mL days)}$, which is a consequence of the homeostatic condition of Equation (16). The renal clearance rate k_{ren} is taken from the parameter estimation performed in [31] and is estimated as $k_{ren} = 10.3\,\text{days}^{-1}$. Particular attention should be paid when estimating the rate of internalisation of G-CSF by the neutrophils. Krzyzanski (2010) [17] measured a value of $0.105\,\text{hours}^{-1}$, while it is estimated in [31] that the maximum Michaelis-Menten elimination to occur at a rate of $4.77\,\text{hours}^{-1}$, and a literature value of 0.015 pM/hour is reported in [35]. The authors of [17] note that their estimate is lower than anticipated. We therefore opted to estimate the rate of internalisation from [31], giving $k_{int} = 114.48\,\text{days}^{-1}$. It is worth noting, however, that model predictions were not significantly different when we used the internalisation rate reported in [17] (not shown). A quasi-equilibrium assumption is used in [17] to calculate the dissociation constant k_D given by $\frac{(C)(R)}{RC} = \frac{k_{on}}{k_{off}} = k_D$, where C is the concentration of G-CSF, R the concentration of G-CSFR receptors, and RC the concentration of receptor complexes in the same manner as in our model by using the law of mass-action (see derivation in [8]). Accordingly we took the dissociation constant they reported and set $k_D = 1.44\,\text{ng/mL}$.

The subcutaneous absorption rate of filgrastim is reported as $0.161\,\text{hours}^{-1}$ in [31] and as $0.651\,\text{hours}^{-1}$ in [17]. As we readapted the latter's absorption model we selected a k_a similar to the value reported therein, namely $k_a = 0.5625\,\text{hours}^{-1} = 13.5\,\text{days}^{-1}$. The bioavailability of filgrastim was found to be dose-dependent in [31]. We estimated $F = 0.602$ from [17], which turns out to be higher than the value found in Figure 3 of [31] who report a value close to $F = 0.3$ based on their model simulations accounting for losses in the subcutaneous tissues. Future work

should address this discrepancy through a sensitivity analysis of our model. Finally, the volume of distribution V_d of filgrastim is set at 1788 mL, between the values used in [31] (1.156 L) and [17] (2.42 L) since both studies utilise V_d in the central compartment only.

Appendix C: PD-related Parameter Estimation

The parameter estimation of the previous section deals solely with the model at homeostasis for a healthy individual. We now turn to the estimation of parameters related directly to the PD effects of zalypsis and filgrastim (the rhG-CSF drug studied). In the absence of data reporting effect versus concentration curves for the mechanism of interest, we derived a theoretical measure for the EC50 values of the Michaelis-Menten equations. In a typical study of saturating effects, we allow for 5% variation in the C_{min} values (starting point) and 15% in the end points C_{max} (saturating concentration). We can equivalently vertically translate the dose-response curve to allow for 0% variation in the start point (implying $C = 0$ gives $E = 0$) and 20% variation in the target endpoint (or that $C = C_{max}$ implies $E > 0.8E_{max}$). In this latter case, the dose-response curve is described by

$$E = \frac{E_{max}C}{EC_{50} + C}. \tag{A4}$$

Let x be the observed effect, which is some fraction of the maximal effect E_{max} so that we report the measured effect as xE_{max}. Then at $C = C_{max}$ we have from Equation (A4)

$$xE_{max} = \frac{E_{max}C_{max}}{EC_{50} + C_{max}} \iff x = \frac{C_{max}}{EC_{50} + C_{max}}$$
$$\iff xEC_{50} = C_{max}(1 - x) \iff EC_{50} = C_{max}\left(\frac{1}{x} - 1\right).$$

Further, suppose that a uniform distribution characterises the variability at the end point, meaning that the probability of reaching $0.8E_{max}$ is equal for each observed dose-response curve. Then by the last equivalency above, we calculate that

$$EC_{50} = C_{max}\left(\frac{1}{0.8} - 1\right) = \frac{C_{max}}{4}. \tag{A5}$$

Practically this indicates that the half-maximal concentration occurs at after the first 25% (quartile) of concentrations in the case of a uniform distribution between dose-response curves. Using this theoretical relationship, we were able to calculate EC50s in absence of clinical data. For our purposes, we express Equation (A5) as

$$EC_{50} = C_{min} + \frac{(C_{max} - C_{min})}{4}. \tag{A6}$$

From the PK model and clinical studies, we are able to measure $C_{min} = G^{homeo}$ and C_{max} and then give an estimate for the half-maximal concentrations which is independent of the target effect. This has the potential to be an important method for the determination of EC50 concentrations when only the PK models are reported. One is also able to attribute other probability distributions at the end points if there is one that is preferable over others. Using Equation (A6) in conjunction with Equation (16), we calculated

$$b_S = b_{NP} = b_{NM} = b_G = C_{min} + \frac{(C_{max} - C_{min})}{4} = 11.2679\,\text{days}^{-1},$$

for the half-maximal concentrations of Equations (19), (20), (21), and (25). The remaining half-maximal concentration parameter relates the effect of G-CSF on the maturation velocity of the marrow neutrophils (Equations (22) to (24)). For this determination, we make use of the data reported in [28, Figure 3] which reports the time-evolution of the appearance of irradiated cells in the circulation after 5 successive days of G-CSF dosing (with daily blood samples and ANC analysis). Assuming the 300 μg dose induced the maximal observed effect, we determined that $V_{max} = 10$ by first calculating the difference that [28] measured for the total production time at the high dose compared to the reported baseline for the whole production time. This difference was then subtracted from our baseline neutrophil maturation time estimation of $a_{NM} = 3.9$. Assuming that the renal elimination is the dominant method of G-CSF excretion during exogenous administration, we can neglect the internalisation elimination and calculate a closed-form solution from

$$\frac{dG_{estimate}}{dt} = \frac{k_a F(Dose_{GCSF})}{V_d} e^{-k_a t_{inj}} + G_{prod} - k_{ren} G(t)$$

to obtain

$$G_{estimate}(t) = \frac{\frac{k_a F(Dose_{GCSF})}{V_d} e^{-k_{ren}t - t(k_a - k_{ren})}}{(k_{ren} - k_a)} + \frac{G_{prod}}{k_{ren}} + e^{-k_{ren}t}\left(\frac{G^{homeo} - \frac{k_a F(Dose_{GCSF})}{V_d}}{(k_{ren} - k_a) - \frac{G_{prod}}{k_{ren}}}\right). \tag{A7}$$

Then, the 30 μg dose is used to find b_V making use of Matlab's $fzero$ function [22] to solve for b_V from Equation (23) (τ_{NM} is determined from the data curve of [28] and a_{NM} is again taken to be 3.9 days). This gave $b_V = 3.5$ ng/mL.

Finally, [32] cite a range of $(8 - 16) \times b_N^{min}$ for their B_N^{max}, which accounts for the maximal birth rate. We take our similar parameter under the cited range since the additional processes of proliferation and maturation accounted for in our model contribute to the 'birth' of neutrophils in our study. With this in mind, we take $trans^{max}$ to be 4 times the homeostatic transition rate, or $trans^{max} = 4trans^{homeo}$.

References

[1] Amgen Manufacturing Ltd. NEUPOGEN-Filgrastim Monograph (2007).

[2] Bernard S, Bélair J, Mackey MC. Oscillations in cyclical neutropenia: New evidence based on mathematical modeling. *Journal of Theoretical Biology* **223**, 283–298 (2003).

[3] Brooks G, Langlois GP, Lei J, Mackey MC. Neutrophil dynamics after chemotherapy and G-CSF: The role of pharmacokinetics in shaping the response. *Journal of Theoretical Biology* **315**, 97–109 (2012).

[4] Cartwright GE, Athens JW, Wintrobe MM. Analytical review: The kinetics of granulopoiesis in normal man. *Blood* **24**, 780–803 (1964).

[5] Colijn C, Mackey MC. A mathematical model of hematopoiesis: II. Cyclical neutropenia. *Journal of Theoretical Biology* **237**, 133–146 (2005).

[6] Dancey JT, Deubelbeiss KA, Harker LA, Finch CA. Neutrophil kinetics in man. *The Journal of Clinical Investigation* **58**, 705–715 (1976).

[7] Foley C, Bernard S, Mackey MC. Cost-effective G-CSF therapy strategies for cyclical neutropenia: Mathematical modelling based hypotheses. *Journal of Theoretical Biology* **238**, 756–763 (2006).

[8] Foley C, Mackey MC. Mathematical model for G-CSF administration after chemotherapy. *Journal of Theoretical Biology* **257**, 27–44 (2009).

[9] Friberg LE, Karlsson MO. Mechanistic models for myelosuppression. *Investigational New Drugs* **21**, 183–94 (2003).

[10] Furze RC, Rankin SM. Neutrophil mobilization and clearance in the bone marrow. *Immunology* **125**, 281–288 (2008).

[11] González-Sales M, Valenzuela B, Pérez-Ruixo C, Fernández Teruel C, Miguel-Lillo B, Soto-Matos A, et al. Population pharmacokinetic-pharmacodynamic analysis of neutropenia in cancer patients receiving PM00104 (Zalypsis). *Clinical Pharmacokinetics* **51**, 751–764 (2012).

[12] de Haas M, van der Schoot CE, Calafat J, Hack CE, Nuijens JH, Roos D, et al. Granulocyte colony-stimulating factor administration to healthy volunteers: Analysis of the immediate activating effects on circulating neutrophils. *Blood* **84**, 3885–3894 (1994).

[13] Haurie C, Dale DC, Mackey MC. Cyclical neutropenia and other periodic hematological disorders: a review of mechanisms and mathematical models. *Blood* **92**, 2629–2640 (1998).

[14] Humphries AR, Craig M, Mackey MC. A mathematical model of myelopoiesis (2015). *In preparation*.

[15] Johnston E, Crawford J, Blackwell S, Bjurstrom T, Lockbaum P, Roskos L, et al. Randomized dose escalation study of SD/01 compared with daily filgrastim in patients receiving chemotherapy. *Journal of Clinical Oncology* **18**, 2522–2528 (2000).

[16] Krinner A, Roeder I, Loeffler M, Scholz M. Merging concepts - coupling an agent-based model of hematopoietic stem cells with an ODE model of granulopoiesis. *BMC Systems Biology* **7**, 117 (2013).

[17] Krzyzanski W, Wiczling P, Lowe P, Pigeolet E, Fink M, Berghout A, et al. Population modeling of filgrastim PK-PD in healthy adults following intravenous and subcutaneous administrations. *Journal of Clinical Pharmacology* **9 Suppl**, 101S–112S (2010).

[18] Layton JE, Hall NE. The interaction of G-CSF with its receptor. *Frontiers in Bioscience* **31**, 177–199 (2006).

[19] Lei J, Mackey MC. Multistability in an age-structured model of hematopoiesis: Cyclical neutropenia. *Journal of Theoretical Biology* **270**, 143–153 (2011).

[20] Mackey MC. Cell kinetic status of hematopoietic stem cells. *Cell Proliferation* **34**, 71–83 (2001).

[21] Madarnas Y, Eisen A, Myers R, Haynes AE. The Prophylactic Use of Filgrastim in Patients with Breast Cancer. Cancer Care Ontario, Toronto, Canada, Program in Evidence-based Care MCED-CCO Special Advice Report 14-2 (2009 Oct 1 (Archived 2013 May)).

[22] Mathworks. MATLAB 2013a. Natick, Massachusetts (2013).

[23] McLennan DN, Porter CJH, Edwards GA, Martin SW, Heatherington AC, Charman SA. Lymphatic absorption is the primary contributor to the systemic availability of epoetin alfa following subcutaneous administration to sheep. *The Journal of Pharmacology and Experimental Therapeutics* **313**, 345–351 (2005)

[24] Pérez-Ruixo C, Valenzuela B, Fernández Teruel C, González-Sales M, Miguel-Lillo B, Soto-Matos A, et al. Population pharmacokinetics of PM00104 (Zalypsis) in cancer patients. *Cancer Chemotherapy and Pharmacology* **69**, 15–24 (2012).

[25] Pfreundschuh M, Trümper L, Kloess M, Schmits R, Feller AC, Rudolph C, et al. Two-weekly or 3-weekly CHOP chemotherapy with our without etoposide for the treatment of young patients with good prognosis (normal LDH) aggressive lymphomas: Results of the NHL-B1 trial of the DSHNHL. *Blood* **104**, 626–633 (2004).

[26] Pfreundschuh M, Trümper L, Kloess M, Schmits R, Feller AC, Rudolph C, et al. Two-weekly or 3-weekly CHOP chemotherapy with our without etoposide for the treatment of elderly patients with aggressive lymphomas: Results of the NHL-B2 trial of the DSHNHL. *Blood* **104**, 634–641 (2004).

[27] Porter CJH, Charman SA. Lymphatic transport of proteins after subcutaneous administration. *Journal of Pharmaceutical Sciences* **89**,

297–310. (2000).

[28] Price TH, Chatta GS, Dale DC. Effect of recombinant granulocyte colony-stimulating factor on neutrophil kinetics in normal young and elderly humans. *Blood* **88**, 335–340 (1996).

[29] Quartino AL, Friberg LE, Karlsson MO. A simultaneous analysis of the time-course of leukocytes and neutrophils following docetaxel administration using a semi-mechanisitic myelosuppression model. *Investigational New Drugs* **30**, 833–845 (2012).

[30] Rankin SM. The bone marrow: A site of neutrophil clearance. *Journal of Leukocyte Biology* **88**, 241–251 (2010)

[31] Scholz M, Schirm S, Wetzler M, Engel C, Loeffler M. Pharmacokinetic and -dynamic modelling of G-CSF derivatives in humans. *Theoretical Biology and Medical Modelling* **9**, 1497–1502 (2012).

[32] Shochat E, Rom-Kedar V, Segel LA. G-CSF control of neutrophils dynamics in the blood. *Bulletin of Mathematical Biology* **69**, 2299–2338 (2007).

[33] Shochat E, Rom-Kedar V. Novel strategies for granulocyte colony-stimulating factor treatment of severe prolonged neutropenia suggested by mathematical modeling. *Clinical Cancer Research* **14**, 6354–6363 (2008).

[34] Vainas O, Ariad S, Amir O, Mermershtain W, Vainstein V, Kleiman M, Inbar O, Ben-Av R, Mukherjee A, Chan S, Agur Z. Personalising docetaxel and G-CSF schedules in cancer patients by a clinically validated computational model. *British Journal of Cancer* **107**, 814822 (2012).

[35] Vainstein V, Ginosar Y, Shoham M, Ranmar DO, Ianovski A, Agur Z. The complex effect of granulocyte colony-stimulating factor on human granulopoiesis analyzed by a new physiologically-based mathematical model. *Journal of Theoretical Biology* **235**, 311–327 (2005).

[36] Wang B, Ludden TM, Cheung EN, Schwab GG, Roskos LK. Population pharmacokinetic-pharmacodynamic modeling of filgrastim (r-metHuG-CSF) in healthy volunteers. *Journal of Pharmacokinetics and Pharmacodynamics* **28**, 321–342 (2001).

[37] Zhuge C, Lei J, Mackey MC. Neutrophil dynamics in response to chemotherapy and G-CSF. *Journal of Theoretical Biology* **293**, 111–120 (2012).